in Table V. A comparison of these expressions including ours with Dewdney's values[15] is shown in Figs. 7 and 9–11. Except for the closed-shell regions, our expressions are in fair agreement with Dewdney's values. Our empirical expression for Z_A with the shell effect terms included [Eq. (12)] is in much better agreement with Dewdney's values than other Z_A formulas none of which contain shell effects on Z_A.

ACKNOWLEDGMENTS

The authors are grateful to Merlin H. Dipert and Angelo Sandrin for computations with the IBM-650 computer, Mrs. Judy D. Varley for computations with the IBM-704 and CDC-3600 computers, Joseph Gvildys for computations with the IBM-704 computer, and George H. Winslow for help in the use of the IBM-610 computer.

PHYSICAL REVIEW VOLUME 136, NUMBER 4B 23 NOVEMBER 1964

Hyperfine Structure and Nuclear Moments of 20.4-Min C^{11}†

R. A. HABERSTROH,* W. J. KOSSLER,‡ O. AMES, AND D. R. HAMILTON
Palmer Physical Laboratory, Princeton University, Princeton, New Jersey
(Received 19 June 1964)

We have measured the hyperfine structure in the $^3P_2$ and $^3P_1$ states of the ground state configuration of C^{11} by the atomic-beam magnetic-resonance technique. The values obtained after corrections for perturbations by nearby fine-structure states are $^3P_2$: $A/h=(-)68.203\pm0.007$ Mc/sec, $B/h=(-)4.949\pm0.028$ Mc/sec; $^3P_1$: $A/h=(-)1.242\pm0.010$ Mc/sec or $(-)1.200\pm0.010$ Mc/sec depending upon the choice of zero-field level ordering, where $B(J=1)=-B(J=2)/2$. From these data it is possible to calculate the nuclear moments of the mirror nucleus, C^{11}, using a theoretical value of $\langle 1/r^3\rangle$ for the p electrons. The results are $\mu_I=(-)1.027\pm0.010$ nm, $Q_{\text{uncorrected}}=(+)(0.0308\pm0.0006)\times10^{-24}$ cm². No signs were measured in these experiments; the indicated signs assume $\mu_I<0$ in C^{11}. A value of 1.5011 ± 0.0006 for g_J was also obtained in the $^3P_2$ state.

I. INTRODUCTION

THE study of the magnetic dipole moments of mirror nuclei should be particularly useful in helping to find good nuclear wave functions. Assuming that these functions are sufficiently well known it may then be possible to check on the form of the magnetic moment operator. Of interest are contributions to this operator from meson currents in the nucleus; these contributions are expected to arise from the exchange of mesons between nucleons (exchange moments) and from the quenching of the anomalous part of the nucleon moment (quenching effects). A theorem due to Sachs[1] states that the exchange moments must be equal and opposite for the members of a mirror pair. A similar theorem should apply to the quenching calculations of Drell and Walecka[2] as they consider only the isotopic vector part of the anomalous magnetic moment. From these considerations it is clear that the sum of the moments of a mirror pair should be more useful in determining the wave function than either of the individual moments. Other effects such as the moment contribution arising from the spin-orbit force must also be taken into account and the reader is referred to Ref. 2 for a further discussion.

Such a program has been carried out for the H^3, He^3 pair resulting in the first direct indication of exchange currents in nuclei,[1] and recently the magnetic moments of the radioactive members of three more mirror pairs have been measured. These nuclei are N^{13},[3,4] O^{15},[5] and Ne^{19};[6] the moments of the stable members are, of course, known. Unfortunately it is not yet possible, for these heavier cases, to do nuclear structure calculations with sufficient accuracy so that the mesonic effects can be detected.

In this paper we report on measurements on the radioactive member of the $A=11$ pair, 20.4-min C^{11}. Previous measurements[7] have determined the spin to be $\frac{3}{2}$. In the next section we shall discuss the necessary hyperfine structure theory. The experimental details are presented in Sec. III, the data and results in Sec. IV, and in Sec. V we discuss the results.

The $A=11$ pair is the first one for which both electric quadrupole moments are now known.

† This work was supported by the U. S. Atomic Energy Commission and the Higgins Scientific Trust Fund.
* Present address: Erstes Physikalisches Institut der Universitaet, Heidelberg, Germany.
‡ Present address: Department of Physics, Massachusetts Institute of Technology, Cambridge, Massachusetts.
[1] R. G. Sachs, *Nuclear Theory* (Addison-Wesley Publishing Company, Inc., Cambridge, Massachusetts, 1953).
[2] S. D. Drell and J. D. Walecka, Phys. Rev. **120**, 1069 (1960).
[3] R. A. Haberstroh and D. R. Hamilton, Bull. Am. Phys. Soc. **7**, 25 (1962).
[4] A. M. Bernstein, R. A. Haberstroh, D. R. Hamilton, M. Posner, and J. L. Snider, Phys. Rev. **136**, B27 (1964).
[5] E. D. Commins and H. R. Feldman, Phys. Rev. **131**, 700 (1963).
[6] E. D. Commins and D. A. Dobson, Phys. Rev. Letters **10**, 347 (1963).
[7] J. L. Snider, M. Posner, A. M. Bernstein, and D. R. Hamilton, Bull. Am. Phys. Soc. **6**, 224 (1961).

II. RELEVANT HYPERFINE STRUCTURE THEORY

The hyperfine structure (hfs) Hamiltonian for an atom with I and $J>\frac{1}{2}$ is given by[8]

$$H_{\rm hfs}=H_{M1}+H_{E2}+g_J\mu_0 H_e J_z+g_I\mu_0 H_e I_z. \quad (1)$$

The first term H_{M1} represents the interaction of the electrons with the magnetic dipole moment of the nucleus and H_{E2} represents the interaction with the nuclear electric quadrupole moment. Magnetic octupole and higher order terms are neglected in this Hamiltonian. This is certainly valid for the accuracy of the C^{11} measurements. The last two terms result from the interaction of the atomic and nuclear magnetic moments with a uniform external field H_e which we take to be in the z direction. See Ref. 9 for a detailed discussion of the calculation of the matrix elements of the hyperfine interaction. In the representation J^2, I^2, F^2, F_z, where $\mathbf{F}=\mathbf{I}+\mathbf{J}$, H_{M1} has the diagonal matrix elements

$$\langle J,I,F,M_F|H_{M1}|J,I,F,M_F\rangle=A(J)C/2, \quad (2)$$

where $C\equiv F(F+1)-J(J+1)-I(I+1)$, and H_{E2} has diagonal matrix elements

$$\langle J,I,F,M_F|H_{E2}|J,I,F,M_F\rangle = B(J)\frac{\frac{3}{4}C(C+1)-I(I+1)J(J+1)}{2I(2I-1)J(2J-1)}. \quad (3)$$

Both the $M1$ and $E2$ operators have off-diagonal matrix elements between different J states in the fine-structure multiplet; thus, small second-order hfs corrections must be included in the calculations.[9] These are shown in Fig. 1.

$A(J)$ and $B(J)$, the hfs constants, are related to the nuclear moments, μ_I and Q, by

$$A=-(\mu_I/IJ)\langle H\rangle_{JJ} \quad (4)$$

and

$$B=eQ\langle\partial^2 V^e/\partial z^2\rangle_{JJ}, \quad (5)$$

where H and V^e are the magnetic field and the electric potential, respectively, produced at the nucleus by the electrons. The notation JJ means that the expectation values are to be computed in the state where $M_J=J$.

The ground-state configuration of the carbon atom is $1s^22s^22p^2$; the resulting levels and their spacings are shown in Fig. 1. Because the fine-structure separations are small, the atoms in the beam were distributed among all the levels so that we were able to make hfs measurements in both the $^3P_2$ and the $^3P_1$ states.

The three hfs separations which were amenable to measurement with the atomic beam apparatus are

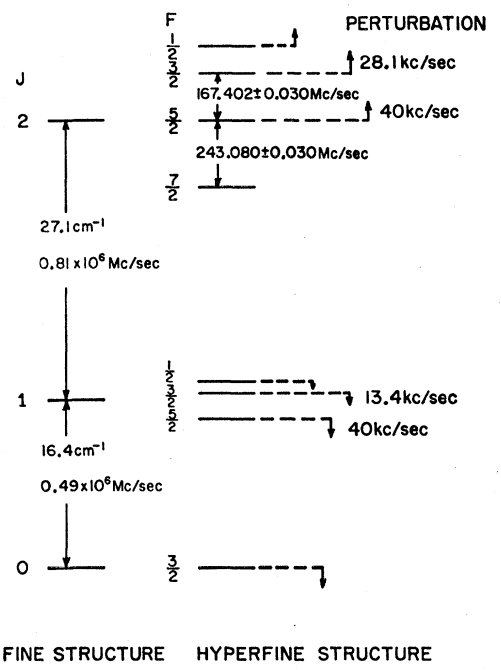

FIG. 1. Energy levels in the ground state term of the C^{11} atom. One of two possible orderings of the F levels in the $^3P_1$ state is shown.

given in terms of the hyperfine constants by

$$h\Delta\nu(\tfrac{7}{2}-\tfrac{5}{2})=\tfrac{7}{2}\{A(^3P_2)+B(^3P_2)/4\} \quad (6)$$

and

$$h\Delta\nu(\tfrac{5}{2}-\tfrac{3}{2})=\tfrac{5}{2}\{A(^3P_2)-B(^3P_2)/4\} \quad (7)$$

for the $^3P_2$ state, and

$$h\Delta\nu(\tfrac{5}{2}-\tfrac{3}{2})=\tfrac{5}{2}\{A(^3P_1)+B(^3P_1)/2\} \quad (8)$$

for the $^3P_1$ state. These results follow directly from (2) and (3).

Because no measured values of A exist for C^{13} it is impossible to deduce the magnetic moment of C^{11} from the formula

$$\left(\frac{IA(J)}{\mu_I}\right)_{C^{13}}=\left(\frac{IA(J)}{\mu_I}\right)_{C^{11}}$$

which follows from (4). We must therefore consider Eq. (4) in more detail. Bessis *et al.*[10] have shown that we may write

$$A(^3P_2)=a_p+a_s, \quad (9)$$

$$A(^3P_1)=a_s, \quad (10)$$

$$A'(^3P_2)=(1/\sqrt{3})(7a_p/6-a_s), \quad (11)$$

$$A'(^3P_1)=(\tfrac{2}{3})^{1/2}(5a_p/6-2a_s). \quad (12)$$

The A' are the off-diagonal hyperfine constants. The term a_p arises from the dipole-dipole interaction of the

[8] N. F. Ramsey, *Molecular Beams* (Oxford University Press, London, 1956).

[9] C. Schwartz, Phys. Rev. **97**, 380 (1955).

[10] N. Bessis, H. Lefebvre-Brion, and C. M. Moser, Rev. Mod. Phys. **35**, 548 (1963).

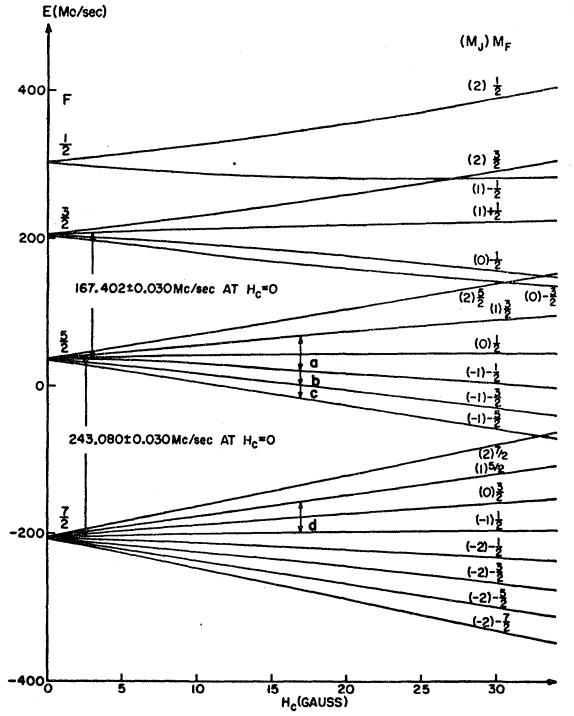

(a)

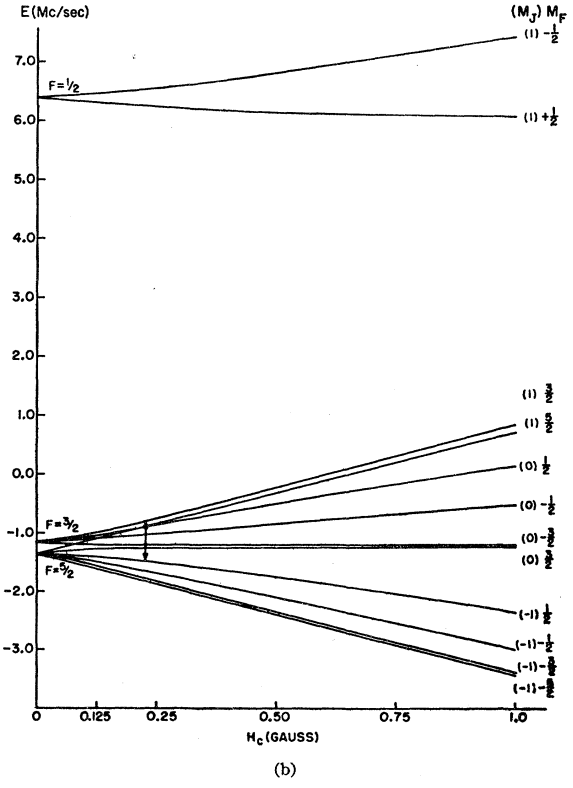

(b)

FIG. 2 (a) Hyperfine structure in the $^3P_2$ state. The resonances observed in the experiment are indicated by the arrows. (b) Hyperfine structure in the $^3P_1$ state. The diagram corresponds to ordering a (see Fig. 9). In the other possible ordering the $F=\frac{5}{2}$ level is 62 kc/sec above the $F=\frac{3}{2}$ level. The arrow shows the direct transition observed in the experiment.

orbital and intrinsic moments of the p electrons with the nuclear magnetic moment and may be written

$$a_p=-\frac{6}{5}\frac{\mu_I\mu_0}{I}\left\langle\frac{1}{r^3}\right\rangle. \tag{13}$$

The term a_s represents the contact interaction between the s electrons and the nuclear dipole moment. That this term should be nonzero for a closed shell is known as the core polarization effect[10–14]; this arises because the radial wave function for an s electron with spin parallel to the p-electron spins will be somewhat different from the radial function of an s electron with spin antiparallel to the p-electron spins. One can either try to compute a_s or, alternatively, measure $A(^3P_1)$ in addition to $A(^3P_2)$, in which case the knowledge of μ_I depends only upon $\langle 1/r^3\rangle$.

It can also be shown for the p^2 configuration that

$$B(J=2)=-(32/5)b_l, \tag{14}$$

where

$$b_l=\frac{3e^2Q}{16I(2I-1)}\left\langle\frac{1}{r^3}\right\rangle.$$

Core polarization will not concern us in the calculation of the quadrupole moment. It will also be useful to use the relation, applicable for this case,

$$B(J=1)=-B(J=2)/2. \tag{15}$$

Detailed hfs level diagrams which we shall refer to later in the text are shown in Figs. 2(a) and 2(b).

III. EXPERIMENTAL PROCEDURES

A. Beam Apparatus

For a detailed description of the atomic beam apparatus see Ref. 4. The most important feature of the machine is that it uses a focusing 6-pole A magnet to polarize the beam and a constant gradient 2-pole B magnet to analyze the beam after the atoms have passed through the radio-frequency loop in the C field. This magnet combination retains the intensity advantage of the Lemonick, Pipkin, and Hamilton machine,[15] in which both A and B magnets are 6-pole and also allows one to have much smaller detecting surfaces and therefore smaller radiation detectors with a consequently significant reduction in background counts.

[11] L. M. Sachs, Phys. Rev. **117**, 1504 (1960).
[12] D. A. Goodings, Phys. Rev. **123**, 1706 (1961).
[13] N. Bessis, H. Lefebvre-Brion, and C. M. Moser, Phys. Rev. **124**, 1124 (1961).
[14] N. Bessis, H. Lefebvre-Brion, and C. M. Moser, Phys. Rev. **128**, 213 (1962).
[15] A. Lemonick, F. M. Pipkin, and D. R. Hamilton, Rev. Sci. Instr. **26**, 1112 (1955).

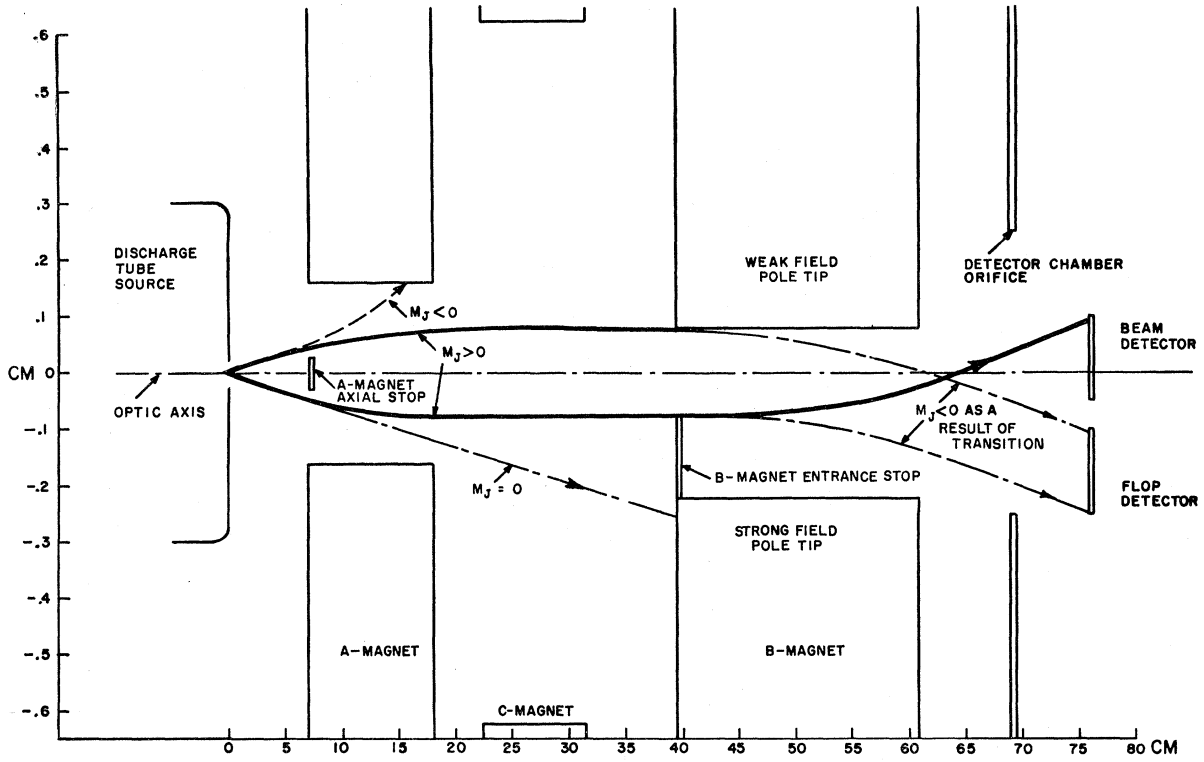

FIG. 3. Horizontal section through machine axis. Note that vertical and horizontal scales are different. Rf loop is not shown.

A diagram of the apparatus is shown in Fig. 3. There are two detector strips; one is positioned to collect those atoms which have undergone a transition ("flopped" atoms), while the other monitors the beam intensity. If F (for flop) and B (for beam) are the counts on each of the detectors for one exposure, then the ratio, F/B, constitutes one datum point. This ratio, rather than F alone, is used to normalize out fluctuations in the beam intensity during a run. The flop detector is sensitive only to transitions for which the sign of M_J changes.

B. Production Technique

Figure 4 shows the technique used for producing the C^{11} beam. Finely divided natural boron powder was sealed in a probe tip and placed in the internal beam of the Princeton FM cyclotron. A beam of 18-MeV protons at a current of about 0.6 μA produced the C^{11} through the reaction $B^{11}(p,n)C^{11}$. Some of the carbon atoms combined with impurities in the probe tip to form gaseous molecules which could then be flushed out. Either neon or helium was used as a flushing gas and it was estimated that about 6% of the C^{11} atoms produced were extracted from the probe tip in this way. The molecules might have been CO; that they were not CO_2 was determined by passing the flow through an ascarite trap; little change was noticed in the amount of activity transmitted. After leaving the probe tip, the activity was flushed through 350 feet of polyethylene tubing to the beam apparatus. A typical transit time was 13 min. Near the beam apparatus, a NaI crystal and count-rate meter was used to monitor the activity in the flow. The transmitted activity showed a pure 20-min half-life. For a typical gas pressure of 1.3 atm at the input to the probe tip, the pressure at the input to the source chamber of the beam apparatus was 4.5 mm Hg. At this pressure a bright discharge could be maintained within the quartz discharge tube which passed through the center conductor of the microwave "tee." The discharge was driven by a QK-61 magnetron (3000 Mc/sec). During all the runs to investigate the $^3P_2$ hyperfine structure research grade neon was used as the carrier gas and it was estimated that about one molecule in 10^3 was dissociated in the discharge. During the $^3P_1$ phase of the work it was found that He gas was more effective in breaking up the molecules by about a factor of 3. Argon gas was also tried, but was only half as effective as the neon. The neon discharge was a good source of metastable atoms which could be used for calibration of the C field during a run. The helium discharge was not as effective in producing He metastables, so that during the runs in which helium was used a small quantity of argon or neon was introduced into the system when it was desired to calibrate the C field. Figure 4 also shows an auxiliary oven used for producing a beam of K^{39}. This was used to check the performance of the apparatus between C^{11} runs.

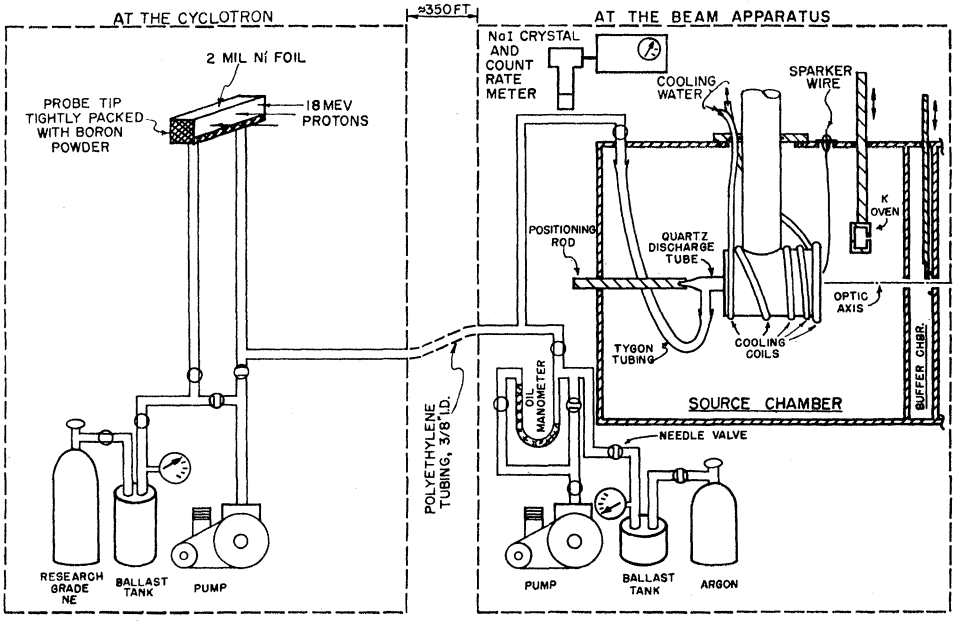

FIG. 4. Technique for producing the C^{11} beam. Just a part of the resonance apparatus is shown. Circle over uninterrupted tubing indicates open valve; over interrupted tubing, closed valve.

C. Detection Technique

The deposition method was used to collect C^{11} atoms. Liquid-nitrogen-cooled silver surfaces were used as the flop and beam detectors. The detector strips were mounted on a copper probe tip which mated snugly with the liquid-nitrogen trap. The silver surfaces were vacuum evaporated onto the detector strips prior to a run.

The collection efficiency was determined by evaporating silver onto a surface and then folding this surface into a box with an entrance aperture exactly the size of a normal collector. Thus an atom which entered the detector box would have to make several wall collisions on the average to escape. If the probability of sticking on the first bounce had been appreciably less than 100%, the box would have been a better collector than a single strip. It was observed that the box had the same efficiency as a single strip so that the collection efficiency was close to 100%.

The collected C^{11} activity was measured by counting the positrons from the predominant decay mode

$$C^{11} \rightarrow B^{11} + \beta^+ + \nu.$$

Following exposure to the beam, the detector strips were removed from the beam apparatus vacuum and were mounted on cylinders which were then seated against two 1-mm-thick plastic scintillators. The counter electronics were standard. The exposure and counting periods for a single datum point were 20 min each in the early phases of the experiment and somewhat less when He was used as the flushing gas. Typical counts above background for 20 min when neon was used as the flushing gas were $F=25$ and $B=750$ with no radio-frequency field. On resonance F increased to about 150 counts. The flop counter was carefully shielded by an inner layer of iron and an outer layer of lead so that the background was about 25 counts in 20 min.

When helium was used as a flushing gas the count rates were two to three times higher than above.

D. Radio-Frequency Techniques

A 16-turn solenoid of Number 18 wire was used as the rf loop and special care had to be taken in its design to avoid the Millman effect.[8] While this effect may be useful in determining the sign of a moment, it can give rise to bizarre line shapes which are often difficult to interpret. The loop was rectangular in cross section, the short dimension in the direction of the C field.

An 8-turn pickup coil was wound on the solenoid and great care was taken during all runs to monitor the amplitude of the rf signal and to use an amplitude appropriate to the quantum multiplicity of the resonance under observation. The amount of rf power needed to attain the first maximum in the transition probability of a resonance in a beam of stable Ar^{40} was used as a reference level for all this work. Because Ar^{40} has no hyperfine structure, this optimum rf power is independent of the value of the static C field, thus making this isotope particularly useful as a calibration. The same, of course, could be said for transitions in Ne^{20} and He^4. The Majorana formula which gives the transition probability as a function of rf field amplitude for these atoms is discussed in detail by Ramsey.[8] Such care was taken because we have found that using excessive rf power can cause severe "pulling" or shifting of a multiple quantum resonance. This effect will be discussed in more detail in the next section.

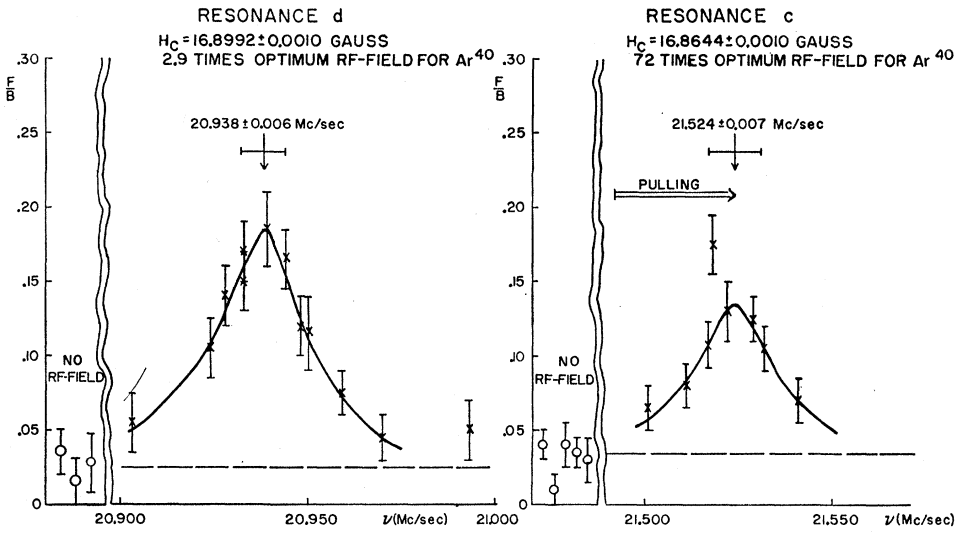

FIG. 5. Two $\Delta F=0$ resonances in the $^3P_2$ state. The amplitude of the rf field needed to induce the transitions is compared with that necessary to induce transitions in stable Ar^{40}.

IV. DATA AND RESULTS

A. Hyperfine Constants in the $^3P_2$ State

The four $\Delta F=0$ transitions indicated in Fig. 2(a) were observed at a static C field of about 17 G. Note that all of these are multiple quantum transitions. It was not possible to observe single quantum $\Delta F=0$ transitions, as J is integral and the beam apparatus is only sensitive to transitions where the sign of M_J changes. Figure 5 shows two of these $\Delta F=0$ resonances. The dashed lines indicate the average of the data points taken with the rf field turned off. The final values of $\Delta\nu$ obtained from the direct $\Delta F=1$ transitions enable us to predict the position of these resonances and the arrow labeled "pulling" on the $4Q$ resonance shows how far it is shifted by the perturbing effect of the large rf field needed to induce the transition. The shift of the 2-quantum resonance is too small to see.

The identification of these resonances was greatly facilitated by the following technique. For a monochromatic beam the transition probability on resonance for an N-quantum transition goes as[16]

$$P=\sin^2\left\{\left(\frac{\text{rf field amplitude}}{\text{optimum amplitude}}\right)^N\frac{\pi}{2}\right\}. \qquad (16)$$

The rf field dependence for an actual resonance will differ somewhat from this form because all the atoms in the beam do not have the same velocity and therefore there is no single amplitude which is optimum for all of them. The result of this is a smearing out of the $\sin^2$ pattern so that after several maxima and minima the curve approaches $P=\frac{1}{2}$, the average of $\sin^2$. The amount of this smearing or damping will depend on the fraction of the velocity distribution transmitted by the apparatus. For our case, the ratio of maximum to minimum velocity is about 1.5, enabling us to see several distinct peaks and valleys. By sitting on the peak of the resonance, then, and varying the amplitude of the rf field, we get a curve which gives us N directly.

The $\Delta F=0$ data are summarized in Table I. These data were used to obtain preliminary values of A and B so that the direct $\Delta F=1$ resonances could be found. The analysis was carried out using the Berkeley "Hyperfine 3–9" program.[17] The four resonances should have been sufficient to yield a value of g_J as well, but there was strong evidence that the 3 and 4 quantum resonances were somewhat shifted in frequency or "pulled."

This perturbation by the rf field may be attributed to two effects. The first, discussed by Hack,[16] is that the rf field will connect the initial (final) state to a state other than the final (initial) state. The second is the Bloch-Siegert effect,[8,18] the basic point here being that the rf field is oscillating and not rotating. The amount of pulling from both these effects goes as the square of the amplitude of the rf field.

We have computed the pulling of the resonances using a program written by Happer,[19] and the results agree well with the experimental shifts which can be

TABLE I. Summary of $^3P_2$ ($\Delta F=0$) C^{11} data. H_c computed from $H_c=\nu(Ne^{20})/[g_J(Ne^{20})\mu_0/h]$ with $g_J=1.500882$.

Resonance	ν (Ne^{20}) (Mc/sec)	H_c (gauss)	ν_{obs} (Mc/sec)
a	35.464±0.002	16.8820±0.0010	23.318±0.006
b	35.489±0.002	16.8939±0.0010	22.450±0.007
c	35.427±0.002	16.8644±0.0010	21.524±0.007
d	35.500±0.002	16.8992±0.0010	20.938±0.006

[16] M. N. Hack, Phys. Rev. 104, 84 (1956).

[17] We wish to thank Professor H. A. Shugart for the use of this program. A description of the program is found in V. J. Ehlers and H. A. Shugart, Phys. Rev. 127, 529 (1962).

[18] F. Bloch and A. Siegert, Phys. Rev. 57, 522 (1940).

[19] W. Happer (private communication).

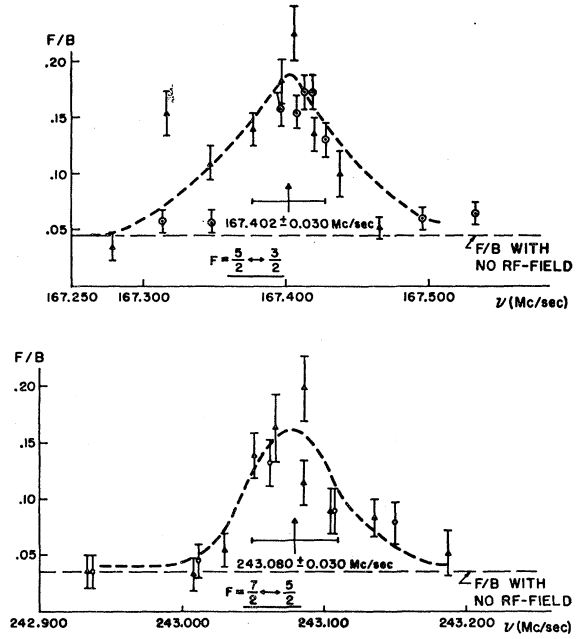

FIG. 6. The $\Delta F=1$ data in the $^3P_2$ state. Different symbols for points indicate separate runs. All frequencies are corrected to zero field.

found after the $\Delta F=1$ transitions have given us the values for $\Delta\nu$.

For the purpose of getting preliminary values of A and B only the two 2-quantum resonances were used since the pulling is negligible for them. A theoretical value of g_J was calculated in a manner similar to that used by Van Vleck[20] for O^{16} and the following rough values for A and B were then obtained:

$$|A(C^{11},{}^3P_2)/h| = 68.16\pm0.50 \text{ Mc/sec},$$
$$|B(C^{11},{}^3P_2)/h| = 4.8\pm1.1 \text{ Mc/sec},$$

and

$$A/B>0.$$

With this information it was then easy to find the direct transitions. These were observed in the Zeeman region, i.e., at a value of H_c of the order of several tenths of a gauss and are indicated in Fig. 2(a). They are $(F,M_F)=(\frac{3}{2},\frac{1}{2})\rightarrow(\frac{5}{2},-\frac{1}{2})$ and $(\frac{5}{2},\frac{3}{2})\rightarrow(\frac{7}{2},\frac{1}{2})$. Figure 6 shows all the $\Delta F=1$ data corrected for the Zeeman splitting so that the peak positions give $\Delta\nu$. The resonances were positively identified by observing how they shifted as the C field was changed. From these curves we have

$$|\Delta\nu(\tfrac{7}{2}-\tfrac{5}{2})| = 243.080\pm0.030 \text{ Mc/sec},$$
$$|\Delta\nu(\tfrac{5}{2}-\tfrac{3}{2})| = 167.402\pm0.030 \text{ Mc/sec}.$$

The final values of A and B were computed from (6) and (7) after making small corrections to the $\Delta\nu$'s for the second-order perturbations caused by states of the same F but different J in the fine structure multiplet. The $^3P_1$ data discussed in the next section were also used in making the corrections. Both the off-diagonal magnetic dipole and electric quadrupole terms were considered. The largest correction was 40 kc/sec, somewhat bigger than the uncertainty in the resonance positions. A negative value of μ_I was assumed in making the corrections. The shifts are shown in Fig. 1. The resulting values of A and B are

$$A(C^{11},{}^3P_2)/h = (-)68.203\pm0.007 \text{ Mc/sec},$$
$$B(C^{11},{}^3P_2)/h = (-)4.949\pm0.28 \text{ Mc/sec}.$$

B. Hyperfine Constants in the $^3P_1$ State

As was mentioned in Sec. II, a determination of the hfs in the $^3P_1$ state will give the term a_s and therefore will remove a source of uncertainty in the calculation of the nuclear magnetic dipole moment.

Figure 7 shows the hfs level ordering in this state as a function of A with B calculated from (15). We shall assume $\mu_I<0$, thus $B(^3P_1)$ is >0. The calculation of Bessis *et al.*[10] suggested an A/h of about -6 Mc/sec and a search was undertaken for a $\Delta F=1$ transition in the region corresponding to this value; no resonance was found. An investigation of the $F=\frac{5}{2}$, $\Delta F=0$ transitions was then begun, and the results suggested an A much nearer to the crossing point of the $F=\frac{5}{2}$ and $F=\frac{3}{2}$ states. It was however, difficult to get much in the way of accurate results from these data because of very large pulling by the rf field. That a large pulling should be expected follows from the fact that the multiple quantum resonances were observed in the $F=\frac{5}{2}$ state with the $F=\frac{3}{2}$ state very close by. Because of this, large amounts of rf power were needed to induce multiple quantum transitions even at low values of H_c. The proximity of the levels resulted in the rf field causing perturbations which were not small compared to the energy of the transition being observed.

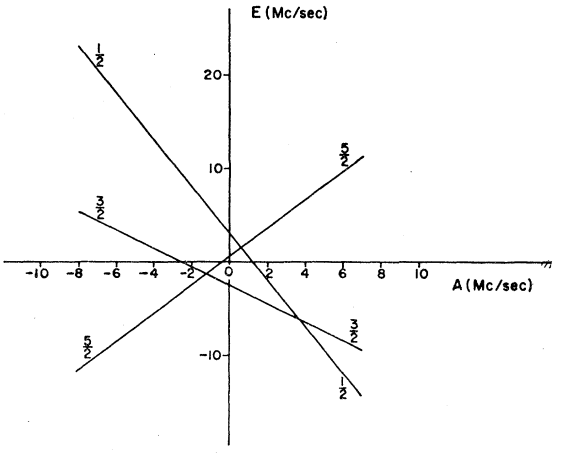

FIG. 7. Zero field ordering of $^3P_1$ hyperfine levels with B chosen to be $+2.4$ Mc/sec.

[20] A. Abragam and J. H. Van Vleck, Phys. Rev. 92, 1448 (1953).

A new search for the $\Delta F=1$ resonance $F=\frac{5}{2}\leftrightarrow\frac{3}{2}$ was carried out at a lower frequency and a typical resonance is shown in Fig. 8(a). Figure 8(b) is a power curve of the type described in Sec. IVA and shows the $\sin^2$ type dependence expected of a 1-quantum transition. The experimental data are summarized in Fig. 9 where the error bars are on the observed resonances. Two values of A, one on either side of the crossing point of the $F=\frac{5}{2}$ and $F=\frac{3}{2}$ states, are consistent with the data. The solid and dashed curves are the computed field dependence of the $\Delta F=1$ resonance for these two choices. The curves marked $^3P_2$ and $^1D_2$ show the positions of the observable $\Delta F=0$ Zeeman transitions in these states. The $^1D_2$ state lies 10 000 cm^{-1} above the ground state and might be populated in the discharge. Note that because the four resonances shown in Fig. 9 are single quantum we may unambiguously identify them as $\Delta F=1$. $\Delta F=0$ resonances must be 2 quantum or higher as discussed in part A of this section. These $\Delta F=1$ resonances must be within the $^3P_1$ hyperfine multiplet because this is the only one populated by the microwave discharge which can have such a small hyperfine splitting. That the transitions must be between the $F=\frac{5}{2}$ and $F=\frac{3}{2}$ levels follows from the fact that the machine optics do not permit a $\Delta F=1$ transition between the $F=\frac{1}{2}$ and $F=\frac{3}{2}$ levels near their crossing point (Fig. 7).

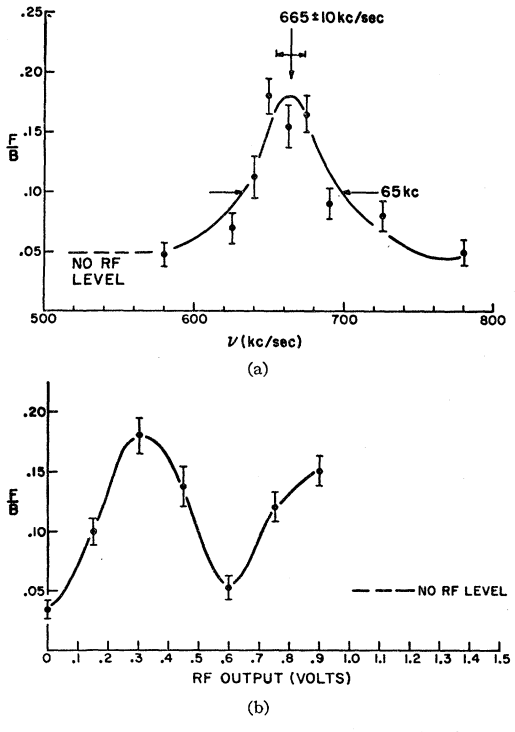

FIG. 8. (a) A $\Delta F=1$ resonance in the $^3P_1$ state. Static C field is 0.214 G. Oscillator output level was 0.3 V. (b) Curve obtained by tuning on the peak of the resonance in Fig. 8(a) and changing the oscillator output. The output is directly proportional to the amplitude of the rf field. The curve illustrates the expected damped $\sin^2$ dependence for a single quantum transition.

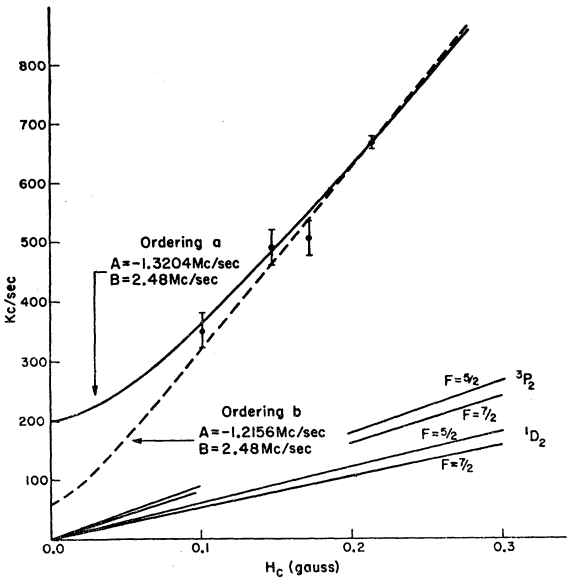

FIG. 9. A summary of the experimental data for the $\Delta F=1$ transitions in the $^3P_1$ state. The solid and dashed curves through the points are theoretical fits. The curves marked $^3P_2$ and $^1D_2$ indicate the positions of the $\Delta F=0$ Zeeman transitions.

Although the two F levels are close together, the pulling is small for these single quantum resonances. Happer's[19] program was used to check this for both choices of A, and the largest predicted shift was 13 kc/sec, somewhat less than the uncertainty in the center of a resonance line.

We now use an average of the two A values found for the purposes of working out the second-order corrections to the hfs splittings in the $^3P_2$ and $^3P_1$ states; the $^3P_2$ results have been given above, the $^3P_1$ results are

$$\Delta\nu(\tfrac{5}{2}-\tfrac{3}{2})=\begin{cases}-0.200\pm0.050\text{ Mc/sec, ordering } a,\\ +0.062\pm0.050\text{ Mc/sec, ordering } b,\end{cases}$$

leading to

$$A(C^{11},{}^3P_1)/h=(-)\begin{cases}1.242\pm0.010\text{ Mc/sec, ordering } a.\\ 1.200\pm0.010\text{ Mc/sec, ordering } b.\end{cases}$$

The value of B is given from (15) and the $^3P_2$ results:

$$B(C^{11},{}^3P_1)/h=(+)2.475\pm0.014\text{ Mc/sec.}$$

C. Nuclear Moments and $g_J(^3P_2)$

From the equations of Sec. II we have computed the nuclear moments for C^{11}. We have assumed the magnetic dipole moment of C^{11} to be <0. This assumption is certainly valid in view of the moment of B^{11}. From Eqs. (9), (10), (13), and (14) and the value of $\langle 1/r^3\rangle=1.1525\times10^{25}$ cm^{-3} calculated by Moser *et al.*[21] we obtain

$$\mu_I=(-)1.027\pm0.010\text{ nm (ordering } a)$$
$$=(-)1.028\pm0.010\text{ nm (ordering } b)$$
$$Q=(+)0.0308\pm0.0006\text{ b.}$$

[21] C. M. Moser (private communication).

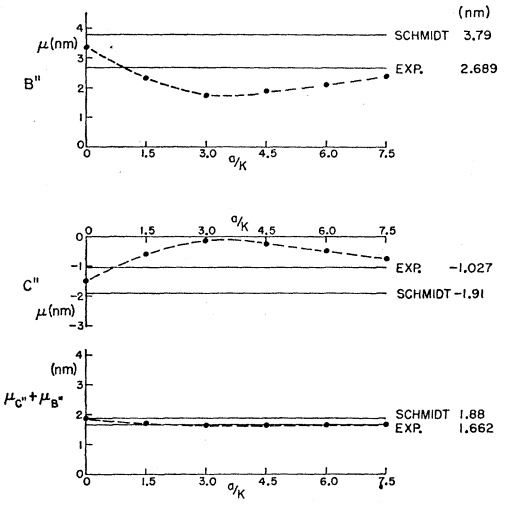

FIG. 10. A comparison of the $A=11$ magnetic moments with theoretical values. Broken lines are from Kurath's intermediate coupling calculations.

The uncertainty in μ_I arises from a somewhat arbitrary 1% uncertainty placed by us on the $\langle 1/r^3\rangle$ value; the uncertainty in Q also includes a possible error of $\pm 1\%$ in the measurement of $B(^3P_2)$. No Sternheimer correction has been made.

From the $^3P_2$, $\Delta F=0$, 2 quantum resonances and the experimental $\Delta\nu$'s we can compute $g_J(C^{11},{}^3P_2)$. This was done using "Hyperfine 3–9"[17] and assuming that $\mu_I<0$. The result is

$$g_J(C^{11},{}^3P_2)=1.5011\pm 0.0006.$$

V. DISCUSSION

The C^{11} nucleus is a particularly difficult case to analyze as we must consider seven nucleons (four protons and three neutrons) in the $1p$ shell. The most extensive calculations in this shell have been performed by Kurath[22] and in Fig. 10 we show his results[23] for the magnetic moments. The number a/K shows the strength of the spin-orbit term in the Hamiltonian. For $a/K=0$ we have pure LS coupling and $a/K=7.5$ represents pure jj coupling. We see that for this case the sum of the moments is worthless in guiding us to any sort of wave function. On the other hand, Kurath has obtained a good fit to the low-lying states in the $A=11$ system by using an $a/K=6.0$. For this value we see that the experimental moments deviate from the theory by about 0.5 nuclear magnetons. It seems clear that considerably more detailed calculations must be carried out before we attribute all or part of such a discrepancy to meson currents. Further calculations[24,25] have been based on a collective model approach. It remains to be seen how useful this will be in the $1p$ shell.

We note that the $A=11$ pair is the first one for which the quadrupole moment of both members is known. As stated above $Q(C^{11})=+0.0308$ b while $Q(B^{11})=+0.036$ b.[26] On a strict single-particle model we would expect the quadrupole moment of C^{11} to be zero, likewise the moment of B^{11} is considerably larger than the single particle value (≈ 0.017 b).

ACKNOWLEDGMENTS

We would like to thank all members of the cyclotron group for their help and understanding during the many hours of running time required to complete this experiment. We are also particularly grateful to Edmond Brower and William Hunt who assisted often during the course of this work and to William Happer who gave us much helpful advice and assistance on the pulling calculations. The calculations were performed on the Princeton University IBM-7090 computer which was made possible by National Science Foundation Grant NSF-GP579.

[22] D. Kurath, Phys. Rev. **101**, 216 (1956).
[23] D. Kurath (private communication).
[24] D. Kurath, Phys. Rev. **124**, 552 (1961).
[25] D. Kurath and L. Pičman, Nucl. Phys. **10**, 313 (1959).
[26] G. Wessel, Phys. Rev. **92**, 1581 (1953).